Karlova Univerzita
Matematicko-fyzikální fakulta
Česká Republika

Studium transportu náboje v amorfním a mikrokrystalickém křemíku s vysokým prostorovým rozlišením

AUTOREFERÁT
DISERTAČNÍ PRÁCE

Mgr. Bohuslav Rezek

Školitel: RNDr. Jan Kočka, DrSc.
Obor: F5, Fyzikální elektronika a vakuová fyzika

Praha, Září 2000

Charles University
Faculty of Mathematics and Physics
Czech Republic

Study of charge transport in amorphous and microcrystalline silicon with high lateral resolution

AUTOREPORT
ON DOCTORAL THESIS

Mgr. Bohuslav Rezek

Supervisor: RNDr. Jan Kočka, DrSc.
Branch: F5, Electronics and vacuum physics

Prague, September 2000

Disertační práce byla vypracována na základě výsledků získaných v letech 1996–2000 v průběhu doktorandského studia na Matematicko-fyzikální fakultě Univerzity Karlovy.

Disertant: Mgr. Bohuslav Rezek
Fyzikální Ústav AV ČR
Cukrovarnická 10
162 53 Praha 6

Školitel: RNDr. Jan Kočka, DrSc.
Fyzikální Ústav AV ČR
Cukrovarnická 10
162 53 Praha 6

Oponenti: Prof. RNDr. Helmar Frank, DrSc.
Fakulta jaderná a fyzikálně inženýrská ČVUT
Trojanova 13
120 00 Praha 2

Doc. Ing. Ladislav Tichý, DrSc.
Společná laboratoř chemie pevných látek
University Pardubice a AV ČR
Studentská 84
532 10 Pardubice

Autoreferát byl rozeslán dne: ....

Obhajoba disertační práce se koná dne: .... v .... hodin před komisí pro obhajoby disertačních prací oboru F5 - Fyzikální elektronika a vakuová fyzika na MFF UK, Ke Karlovu 3, Praha 2, v místnosti č. ....

S disertační prací je možno se seznámit na oddělení doktorandského studia MFF UK, Ke Karlovu 3, Praha 2.

Předseda oborové rady F5: Prof. RNDr. Vladimír Matolín, DrSc.

Acknowledgements

First of all I would like to thank Dr. Jan Kočka, my supervisor and head of the Thin Films department of the Institute of Physics in Prague who has kindly offered me a unique occasion to perform this work in his research group. He gave a place, sense and future prospects to my research in photovoltaics and physics in general. He helped me by many comments and advices during my work.

I would also like to thank Prof. Martin Stutzmann, head of the Experimental Semiconductor Physics department in Walter Schottky Institut in Munich, who has made possible my research stay within his group. The stay in Munich has brought me much experience, both scientific and personal, and turned out to be very fruitful and successful.

Dr. Antonín Fejfar and Dr. Christoph Nebel have been very motivating persons to collaborate with who were able to share their enthusiasm and experience. They helped me a lot with their scientific competence and their ability to present the essential points in a very clear way. They devoted their time for open discussions, allowing me to propose and develop my own ideas. Especially, they also encouraged me in times when I was in doubt.

I gladly acknowledge a friendly cooperation and assistance of Christopher Eisele, who put a great effort into setting up and fine tuning the LBIC setup and who by many small things made my dwelling in Munich so unique experience. I am no less grateful to the other members of the Walter Schottky Institut team for their welcome and assistance.

I want to express many thanks to Ing. Jiří Stuchlík who was in charge of the *in-situ* a–Si:H/μc–Si:H technology and prepared with a great patience and care all PECVD samples.

My grateful thanks go also to Dr. Vladimír Cháb and Dr. Michal Ondřejček who helped me with STM and AFM operation and with understanding of the sensitive world of surface physics. Consultations with Dr. Ivan Ošťádal were of much help to me, especially in the initial stage of my study.

The creative and friendly ambience of the the Thin Films department has been great to dwell in. All my colleagues and friends in the group deserve a special thank as individuals for the good time I have spent in their company.

Last but not least, I would like to thank my parents who in many ways supported me in the course of my post-graduated studies.

1. Introduction

Among all semiconductors, silicon has found unprecedented large-scale use in electronic devices of all kinds. Monocrystalline silicon is commonly used in integrated circuits due to its excellent electronic properties. Deposition of silicon in thin films would be preferred in solar cell industry. It can be deposited directly on large substrates and material consumption as well as production costs are reduced. The low cost of solar energy can decrease the share of fossil fuel powerplants on energy production and thus reduce pollution of our environment.

However, on low cost substrates such as glass or polymer foils, silicon thin films can be grown only in amorphous or microcrystalline form up to now. Although they absorb the light stronger, their electronic transport properties do not reach the quality of monocrystalline silicon. Since amorphous silicon suffers from degradation induced by illumination (Staebler-Wronski effect [?]) the research focus has moved to microcrystalline silicon in the recent years.

Widely used techniques for preparation of microcrystalline silicon are plasma enhanced chemical vapour deposition (PECVD) and laser crystallization of amorphous silicon thin films. The average grain size achieved by conventional PECVD remains in the range of several tens of nanometers, which limits mobility of charge carriers to about 1 cm^2/Vs compared to 1300 cm^2/Vs in monocrystalline silicon. Pulsed interference laser crystallization (ILC) has been recently introduced as a cheap and fast technique to produce large grained silicon thin films [?] as well as higher efficiency a–Si:H based solar cells with structured microcrystalline silicon contact [?].

The thin film deposition processes frequently do not result in uniform homogeneous layers. The initial nucleation of the film on the substrate and the subsequent pattern of growth can cause microscopic inhomogeneities, such as voids, columnar structures and surface roughness. Moreover, microcrystalline silicon is an inherently inhomogeneous material by itself. It consist of crystalline grains separated by grain boundaries, where most of the electronic defects is supposed to be located [?]. In the initial stages the growth gradually develops from amorphous to microcrystalline [?]. This transition layer presents a basic problem for microcrystalline silicon based solar cells because its series resistance decreases the cell efficiency [?]. The coexistence of microcrystalline silicon grains, grain boundaries and amorphous tissue together with columnar growth results in complicated microstructure, which may lead to anisotropy in the transport properties [?].

While the macroscopic properties of microcrystalline silicon layers are relatively well characterized very little is known about their properties on a microscopic scale because standard macroscopic techniques can give only average values of important transport quantities in such an inhomogeneous material.

The main aim of this thesis is to investigate various ways how to find the missing connection between the thin film microstructure and the electronic transport properties. One approach is to use inherently microscopic techniques, of which scanning tunneling microscopy (STM) or atomic force microscopy (AFM) are main representatives [?, ?], and to combine them with the detection of particular quantities of interest in parallel to standard surface morphologies. In contrast to the STM, which detects the tunneling current, the atomic force microscopy (AFM) senses forces between the tip and the sample. While reliable use of electron tunneling is limited to the materials with high enough conductivity, detection of interaction forces can provide surface morphology and electronic properties on any sample of interest.

Another possibility is to modify the macroscopic characterization methods to probe the material properties locally with as high lateral resolution as possible. For instance a technique of electron/light beam induced current (EBIC/LBIC) gives rise to spatially resolved photocurrents by scanning with a focused beam [?, ?].

2. Probing with a point contact

In studies of initial stages of growth of μc–Si:H prepared by PECVD and for investigation of laser patterning of amorphous silicon layers, ultra high vacuum AFM by Omicron Vakuumphysik was employed. The AFM was operated in contact mode and conductive cantilevers were used to provide a point contact to the sample. The cantilevers (produced by Nanosensors) were made of highly p-doped silicon coated with platinum-iridium (PtIr) or p-doped diamond layer. Although PtIr coated cantilevers required more care, because wear of the coating at the very tip may occur [?], both types of cantilevers were found to provide qualitatively same images of local currents and morphology.

The normal force acting on the cantilever was calculated from the deflections by using a known spring constant of the particular cantilever. The image of the surface morphology is then rendered by following the profile of constant cantilever deflection, i.e. constant force. In the constant force regime the cantilever tip is kept in close mechanical and thus also electrical contact with the sample. To obtain maps of local currents at the same time a dc voltage was applied to the bottom sample electrode

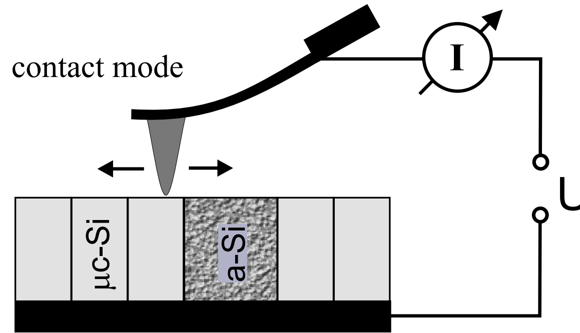

Figure 1: *The schematic drawing of the AFM contact mode operation in a regime, where both surface morphology and local currents are registered simultaneously. The surface morphology is rendered by scanning the profile of constant force while the current is acquired by application of a bias to the conductive cantilever.*

and the current was registered by the cantilever. This arrangement is illustrated in Fig. ??. In this manner, transport and structural properties can be directly compared with each other.

This method has also an advantage of characterizing transport perpendicular to the substrate (i.e., the direction of charge collection in solar cells), unlike many other transport characterization methods using coplanar electrodes [?, ?].

Lateral resolution of surface morphology in contact AFM is determined by the effective area of the tip-sample contact. Simple continuum models were found to give a reasonable description of the mechanical behaviour of the elastic contact between an AFM tip and a smooth sample surface [?]. In a local current measurement, resolution is limited by an effective electrical contact, which has no simple relation to the effective mechanical contact. The current can in principle consist of two components: a current determined by the resistance of the intimate contact and a tunneling across the peripheral region of small separation. On corrugated surfaces, the effective contact is affected by morphological features.

Quality of the surface is also important, because the local electrical contact can be influenced by adsorbates and thin layers covering the surface, such as SiO_2. AFM operation under ultra high vacuum and the *in-situ* sample deposition were found necessary for good electrical contact and well defined surface properties. After the deposition, the PECVD samples were transferred into the measurement chamber without breaking vacuum ($p < 10^{-7}$ mbar). Although morphology measurement was possible in air, the measurement of local currents was unstable, most likely due to unstable environment conditions and surface oxidation.

Measurement of local current can be performed in two distinct regimes. In so called spectroscopic regime, AFM feedback control is switched off after measurement

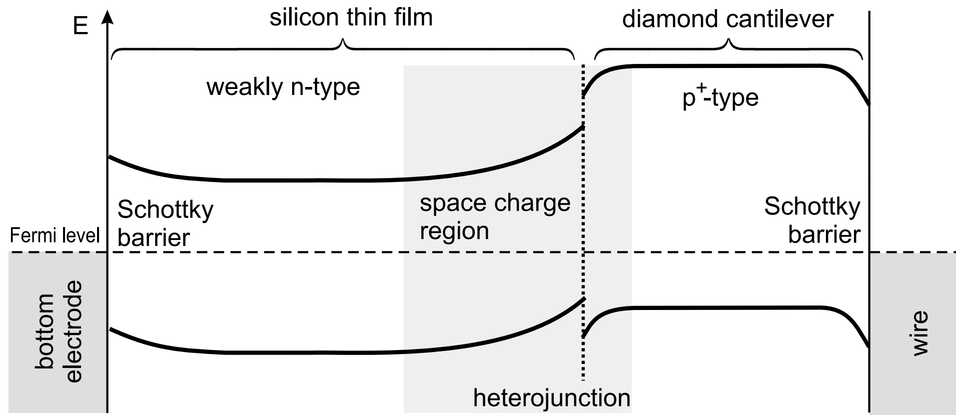

Figure 2: *The schematic drawing of the contact barriers and junctions involved in combined AFM on intrinsic, weakly n-type sample (for instance a–Si:H). Note the hetero-junction between silicon (E_g=1.1–1.7 eV) and diamond coated cantilever (E_g=5.4 eV). The energy gap width is not in scale.*

of surface morphology at a particular point, a voltage is applied to the cantilever and the current is registered. This method of operation has an advantage of a full control over the current measurement timing. When surface morphology and local current are registered simultaneously, a bias voltage is applied permanently as the image is rendered. Simultaneous regime is faster and more straightforward since it avoids voltage pulses used in spectroscopy.

Since the sample structures and probing tips incorporate both metals and semiconductors of various doping type and doping level, space charge regions are formed at their junctions, which gives rise to transport barriers in the measurement circuit. Schematic drawing of the case, where *in-situ* prepared a–Si:H layer (no SiO_2 layer on top) is probed by a diamond coated cantilever, is shown in Fig. **??**. There is a band bending at both electrode/a–Si:H and a–Si:H/cantilever interfaces in order to equilibrate Fermi levels. Another Schottky barrier builds up at the connection of the cantilever to the rest of the circuit.

Laser patterning of amorphous silicon

After comprehensive analysis of capabilities and constraints of the local current measurement in atomic force microscope, the technique of combined AFM/current measurement was applied to investigate microcrystalline silicon patterns prepared by interference laser crystallization of hydrogenated amorphous silicon (a–Si:H).

To produce the patterns on microscopic scale, a–Si:H layer of 200 nm thickness was used. It has been prepared by radio frequency PECVD technique (13.56 MHz, 8 % silane dilution in hydrogen) on Corning 7059 glass substrate covered with semitrans-

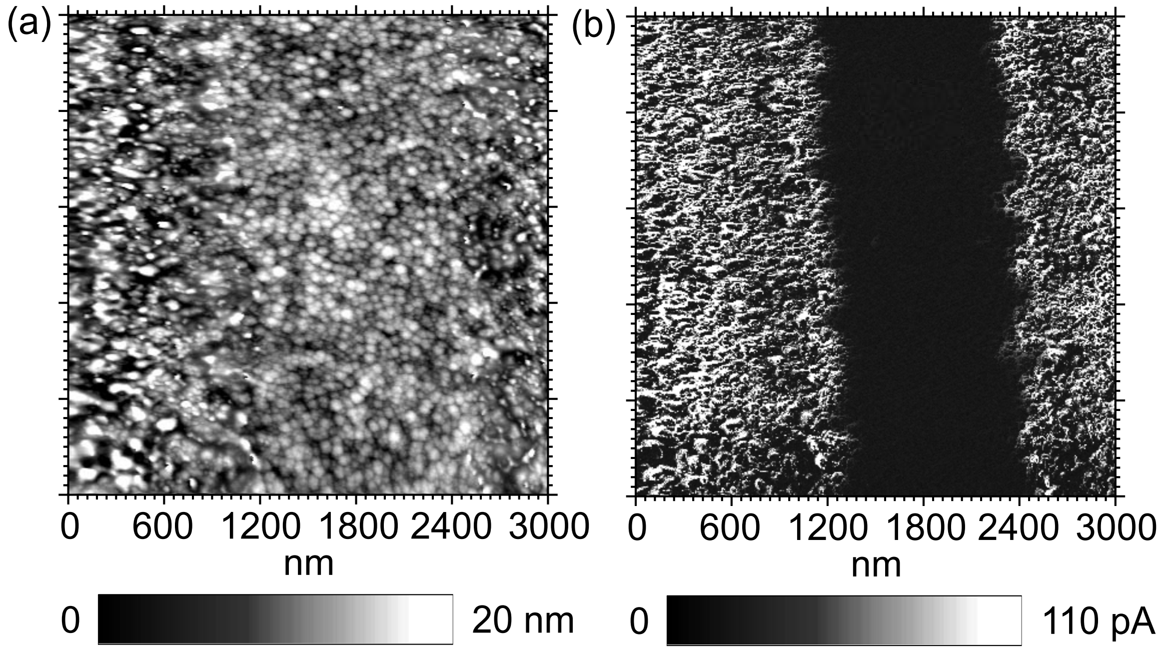

Figure 3: *(a) AFM surface morphology of the laser patterned a–Si:H and (b) the map of current flowing between the cantilever and the bottom ITO electrode in which microcrystalline and amorphous areas are clearly distinguished.*

parent indium tin oxide (ITO) electrode. Prior to the laser crystallization, hydrogen has been effused in vacuum by heating up the samples to 450°C for 1 hour. Effused samples have been crystallized in air by a single pulse of frequency doubled Nd:YAG laser with wavelength 532 nm and energy density 80 mJ/cm^2. Primary laser beam was split in two beams, which overlapped on the sample and formed an interference pattern with period of 5.3 μm. This setup resulted in creation of parallel stripes of amorphous and microcrystalline silicon.

The surface morphology of the layer after laser patterning as measured by AFM using a platinum coated cantilever is presented in Fig. **??**(a). However, it is not easy to distinguish amorphous and microcrystalline parts there. Although microcrystalline silicon part can be visualized by selective etching, this is an additional technological step which can modify the laser induced patterns. On the other hand, measurement of the local conductivity through the layer in parallel to standard AFM picture is a non-invasive probe, which can be used also *in-situ*. Local current measurement has been performed in the spectroscopic regime. In each point the current was averaged for 640 μs with 800 μs delay after the dc voltage of -5 V was applied to the cantilever. Resulting local current map shown in Fig. **??**(b) clearly resolves two types of materials and reveals the exact position and shape of boundaries between amorphous and microcrystalline areas. Being the conductivity of microcrystalline silicon higher than

the one of amorphous silicon, the dark low conductive area in Fig. ??(b) is assumed to correspond to the amorphous tissue while brighter areas, exhibiting much higher currents, are associated with microcrystalline material.

Since the laser processing was done in air, the sample was exposed to the ambient oxygen and thin natural SiO_2 layer most likely developed on the sample surface. Although the thin oxide layer represents an electronic barrier, the material contrast could still be achieved. Obviously the local currents are controlled by the electronic properties of material itself.

Initial stages of μc–Si:H growth

The substrate, on which μc–Si:H is grown, is known to exhibit a strong influence on the resulting layer structure. Using combined AFM/current measurement, the effect of metallic, device quality a–Si:H and laser annealed a–Si:H substrate layers on further μc–Si:H growth was studied.

To investigate growth on metallic layer, which is often used as a contact, a thin layer of μc–Si:H was deposited on a nickel-chromium (NiCr) electrode, which had been evaporated on a Corning 7059 glass substrate. The 100 nm thin layer of μc–Si:H was grown by radio frequency PECVD technique using 4 % dilution of silane (SiH_4) in hydrogen.

AFM surface morphology and local current image of this layer are shown in Fig. ??. The images were obtained simultaneously using platinum coated cantilever and 3 V bias voltage between the bottom electrode and the cantilever. The surface morphology, which is represented by normal force image in Fig. ??(a), is homogeneously populated by rounded formations of similar size and shape. Obviously the NiCr electrode provides an abundant amount of nucleation centers. The picture of homogeneous material is ruined by the map of local currents in Fig. ??(b), which clearly shows a large number of the silicon crystallites on the surface together with still amorphous material. From the area occupied by the crystallites the fraction of crystalline material could be estimated to about 78 %.

For comparison, a–Si:H was grown in the same manner, except the silane dilution of 8 % being used. Although purely amorphous layer looks similar in morphology to μc–Si:H no features in local current were observed.

To study a–Si:H/μc–Si:H interface, which plays an important role in solar cell technology, specific samples were prepared. The primary substrate was again NiCr electrode evaporated on a Corning 7059 glass. But now prior to the deposition of

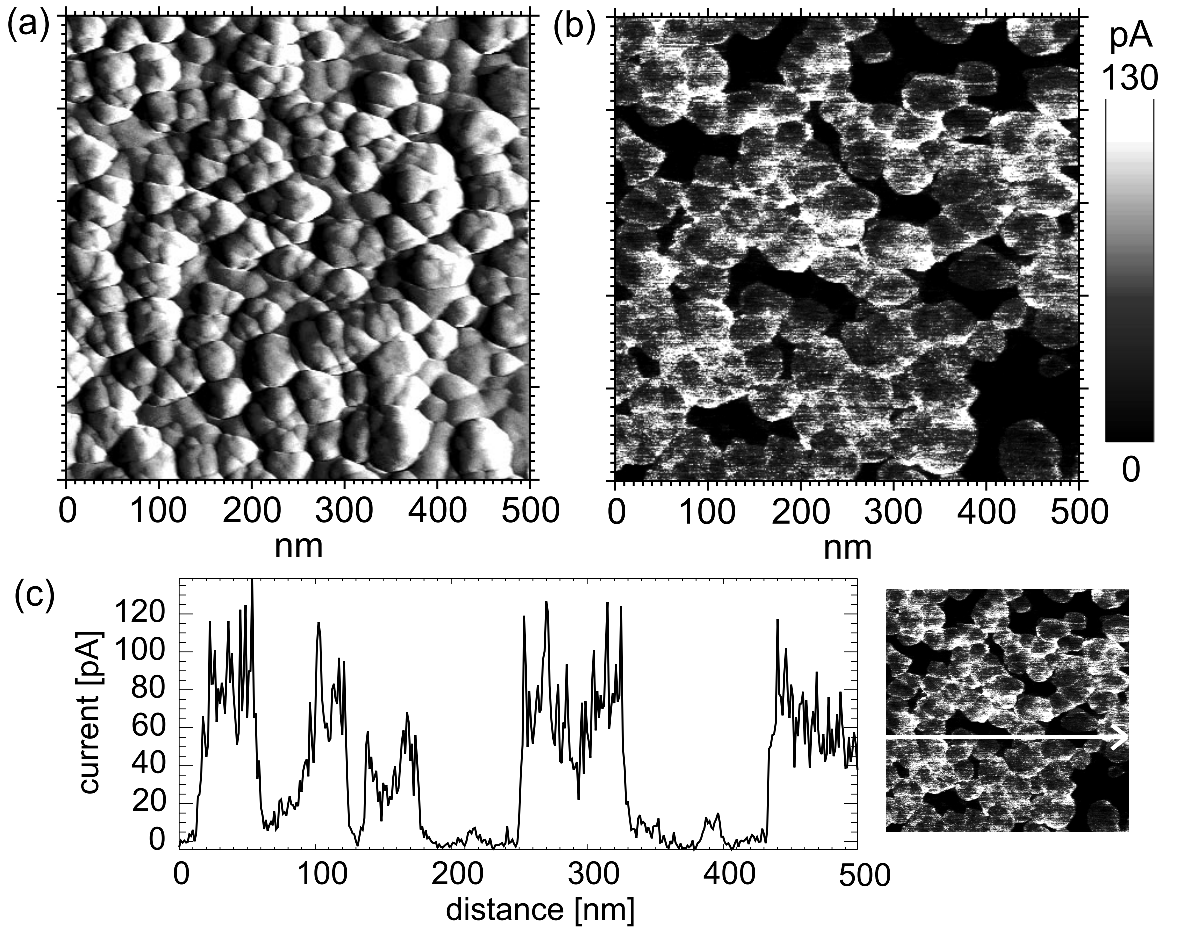

Figure 4: *(a) AFM surface morphology represented by normal force image and (b) local current image of 100 nm μc–Si:H layer upon NiCr electrode biased at 3 V. (c) The current spatial profile measured across the sample as indicated by the white arrow in the small image on the left. While the layer appears homogeneous in surface morphology, the local currents reveal that part of the layer is still amorphous.*

μc–Si:H, 100 nm layer of hydrogenated amorphous silicon was first deposited on the substrate using 8 % dilution of silane in hydrogen. Then the deposition continued under conditions readjusted for μc–Si:H growth by changing silane dilution to 4 %. The a–Si:H and μc–Si:H layers made up the total sample thickness of 540 nm.

AFM surface morphology and current map of the μc–Si:H grown on the amorphous substrate layer were obtained using platinum coated cantilever and 3 V bias voltage between the cantilever tip and the bottom electrode. The results are shown in Fig. **??**. In the surface morphology shown in Fig. **??**(a), roughly circular protrusions can be resolved above the smoother and relatively flat rest of the surface. The larger protrusions seem to be composed of finer grains with sizes around 20 nm. These protrusions were assumed to correspond to the surface of the silicon crystallites and crystalline columns surrounded by the amorphous matrix. This assumption was clearly proved by the local current map in Fig. **??**(b) and the current spatial profile in

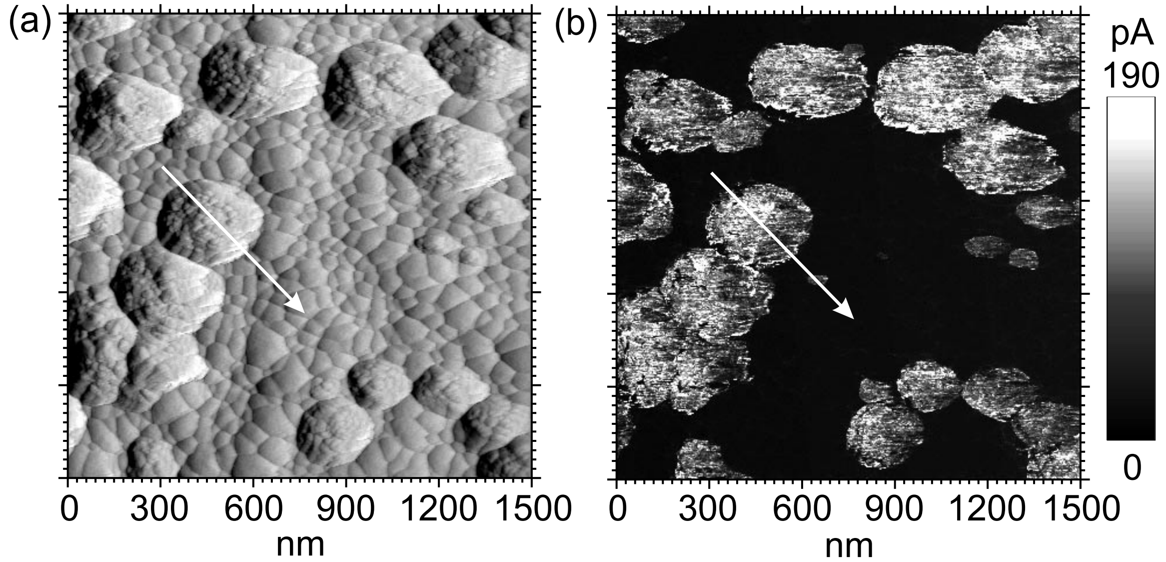

Figure 5: *(a) Surface morphology of the μc–Si:H layer grown on 100 nm a–Si:H obtained using AFM with a platinum coated cantilever and 3 V bias voltage. The morphology is represented by the normal force image. (b) The map of simultaneously measured local current flowing between the cantilever and the bottom NiCr electrode. Microcrystalline areas are clearly resolved against the dark (less conductive) amorphous background. The lines indicate the location of the profiles shown in Fig.* **??**.

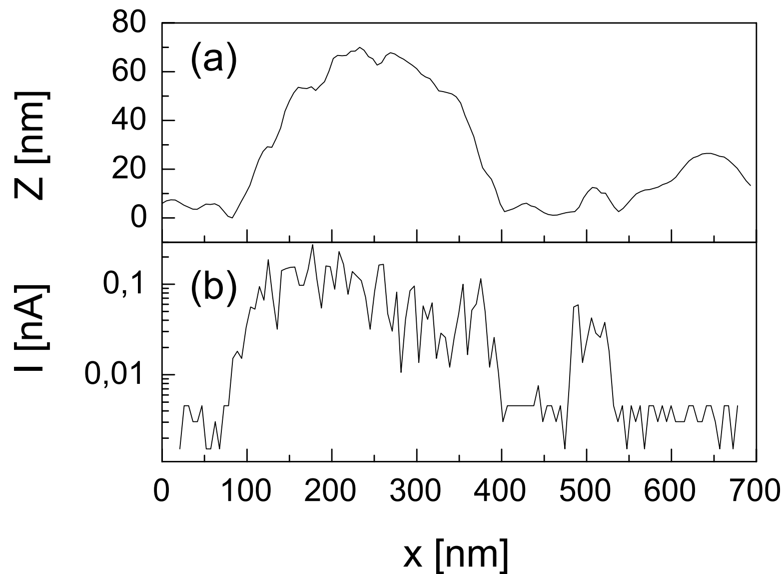

Figure 6: *Profiles of the sample surface height (a) and local current(b) along the lines depicted in Fig.* **??**. *Even very small crystallite at $x = 500$ nm which would pass unnoticed in the morphology can be identified in the current.Although a peak is observed in sample height at position around $x = 650$ nm, the current remains low, indicating an amorphous region.*

Fig. ??(b), which shows that the local current is much higher on the protrusions than on the rest of the sample. This is in agreement with expected higher conductivity of μc–Si:H in comparison to a–Si:H.

The reliability of the crystalline area identification is illustrated by comparison of the height and current spatial profiles in Fig. ??. They pass through one large and one small protrusion as represented by the arrows in Fig. ??. Even very small crystallite at $x = 500$ nm which would pass unnoticed in the morphology can be identified in the current. On the other hand, although a peak is observed in sample height at the position around $x = 650$ nm, the current remains low, indicating an amorphous region. The large irregularities of the current observed on top of the crystallites are most likely because these crystallites are assembled from fine crystalline grains. The observation of both μc–Si:H and a–Si:H material in AFM local current images of the layers is corroborated by the measurement of constant photocurrent method.

The crystallinity of the layer is reduced to 40 % compared to the crystalline fraction of 78 % found in μc–Si:H, which was grown directly on NiCr substrate. Obviously the a–Si:H substrate layer inhibited the nucleation and retarded the development of the μc–Si:H layer.

The retarded development of crystallinity of μc–Si:H layer can present a problem in a–Si:H/μc–Si:H devices. To alter nucleation conditions, the a–Si:H substrate layer was annealed by laser irradiation prior to the subsequent deposition of μc–Si:H. The laser annealing was done inside the deposition chamber by a single pulse of ArF excimer laser with wavelength 193 nm and energy density 80 mJ/cm^2, which is just above the a–Si:H melting threshold.

As shown in Fig. ??, both the surface morphology and current map are substantially different for the sample in which the amorphous substrate layer was annealed by laser. In this case very high fraction of crystallites and negligible amorphous tissue is observed on the surface. The crystallinity estimated from the current map reached about 95 %.

The estimates of the crystallinity were verified by Raman scattering. The spectra were measured on the samples with a–Si:H substrate layer using argon laser excitation with short penetration depth, so that crystallinity on the surface is evaluated. The crystallinity was simply deduced from the ratio of Raman intensity at 520 and 480 cm^{-1}. The results 56 % and 88 % are in qualitative agreement with the values found from the local current images. Raman spectra also indicated that laser irradiation of the a–Si:H substrate layer by one pulse creates a very defective a–Si:H layer instead of crystallization of the amorphous layer [?]. The numerous defects

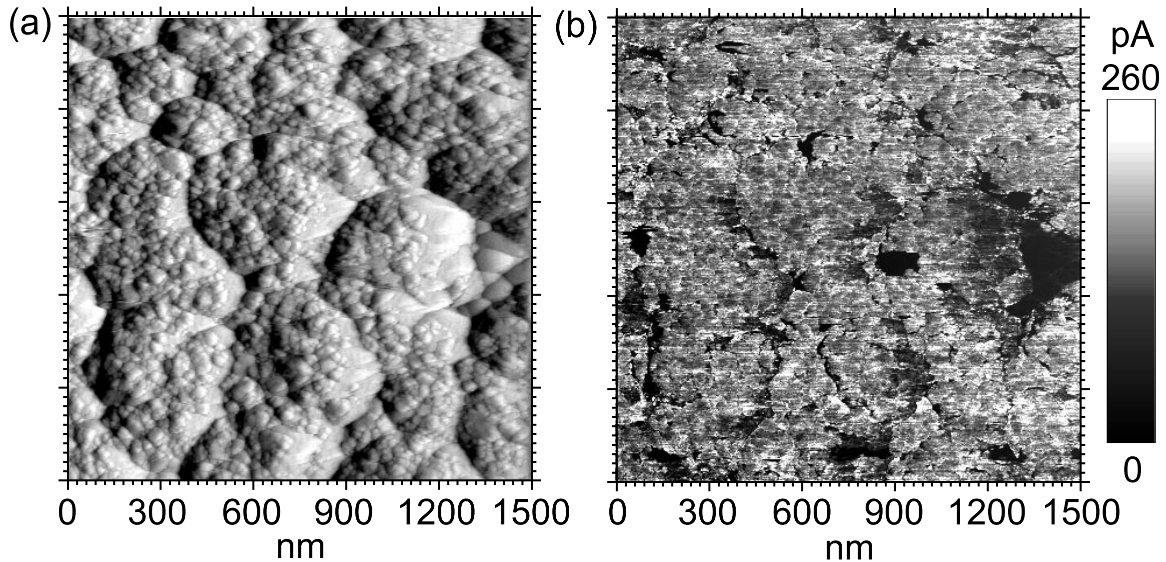

Figure 7: *(a) AFM surface morphology represented by normal force image and (b) the map of local current of the μc–Si:H layer grown on laser annealed a–Si:H substrate layer. The images were obtained using AFM with a platinum coated cantilever and 3 V bias voltage. The sample was grown in the same deposition as the sample shown in Fig.* **??***, the only difference is that the a–Si:H substrate layer was treated by a single excimer laser pulse in this case.*

obviously acted as additional nucleation centers and resulted in higher crystalline fraction.

Memory effect in local current

In the course of local current measurements, silicon thin films were found to remember that the voltage was applied at a particular place. This observation is demonstrated by Fig. **??**(a), where 1500 × 1500 nm image of local currents on 100 nm thin layer of μc–Si:H was acquired using a platinum coated cantilever at 4 V bias. A dark square area, dimensions of which are approximately 500 × 500 nm, appears in the center of the image. The dark area exhibits overall lower conductivity than the rest of the sample as shown in the current spatial profile in Fig. **??**(b). This is the result of a previous AFM/current measurement at that place. Prior to the measurement of 1500 × 1500 nm area in Fig. **??**, the 500 × 500 nm area was already scanned several times at the same bias of 4 V, so that each measurement point was exposed to the bias voltage for the total of 15 ms compared to 5 ms in the outer region. The decayed area persists on the surface for at least several hours.

In amorphous or microcrystalline silicon, this decay is likely connected with the transient depletion of electrons from deep states, the concept of which was introduced

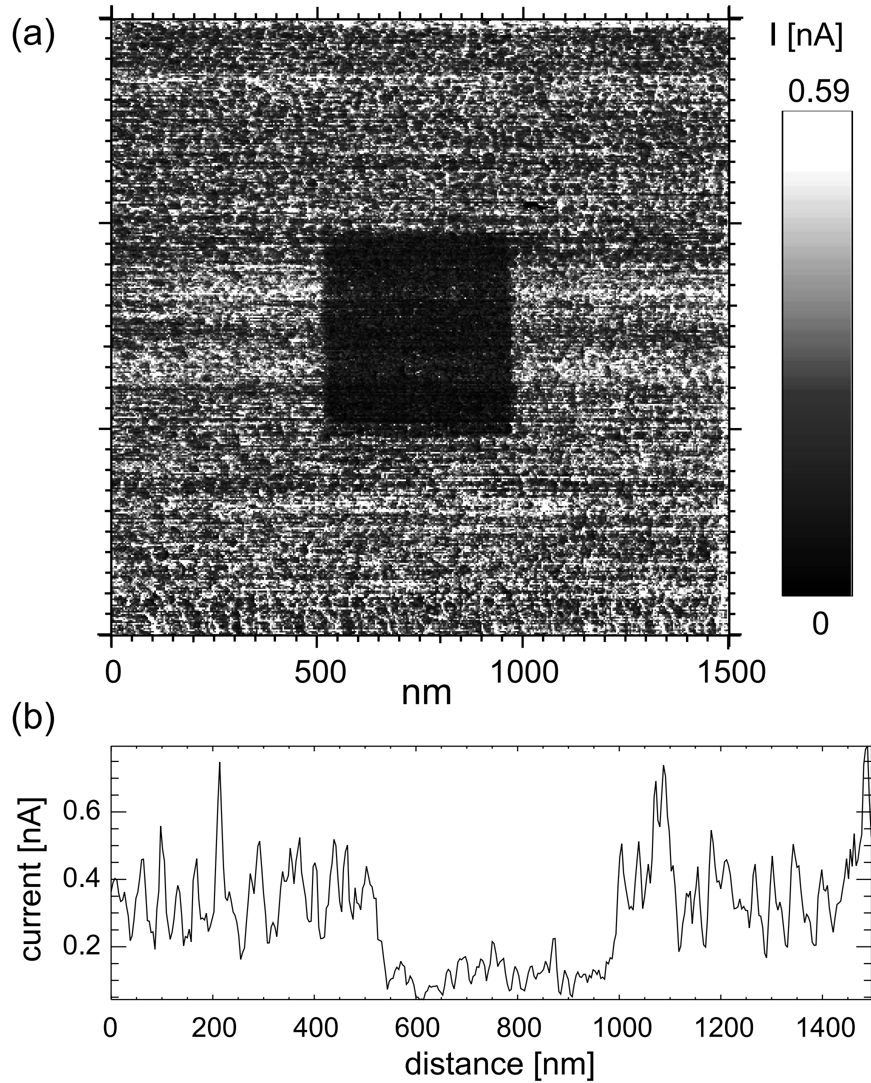

Figure 8: *(a) Image of local currents acquired at 4 V bias on 100 nm thin μc–Si:H layer with a NiCr bottom electrode. The dark, low conductive square area in the center is a result of previous current measurement, which was scanned at that area prior to acquisition of this image. (b) The current spatial profile clearly shows overall reduced current amplitude in the dark region.*

by Street [**?**]. When a conductive cantilever is brought into contact with amorphous or microcrystalline silicon layers, there is a transfer of charge across the interface to bring the two Fermi levels into alignment and achieve thermal equilibrium. The resulting contact exhibits rectifying electrical properties. After application of a reverse bias voltage, there is a thermally generated transient release of depletion charge from gap states to achieve new equilibrium. This results in a pronounced decay of reverse current over long period of time.

Although the complete mechanism of this memory effect is still unknown, it may show up as an interesting feature for application in microelectronics and is worth of further investigation.

3. Probing with a focused laser beam

Photoelectrical properties of microcrystalline silicon thin films are of high importance for making use of the material in solar cells and other devices. Their quality can be evaluated by application of laser beam induced current (LBIC) technique.

Principle of the laterally resolved LBIC measurement is simple as shown in Fig. ??. The sample is illuminated by a focused laser beam. As the focus spot is scanned by piezo drives across the sample between the electrodes, photocarriers are generated locally and resulting photocurrent is registered by lock-in technique. External bias is usually applied to extract the photocarriers, however, the built-in fields may be probed also without a bias.

The spatial resolution of the LBIC setup was determined by moving the focus spot over the edge of a metallic layer, below which a large area photodiode was positioned. The intensity profile is approximately gaussian with a typical diameter (I_{max}/e^2) of about 0.8 μm. Considering the Rayleigh criterion, an electronic resolution of approximately 0.4 μm is expected.

The LBIC technique was applied to microcrystalline silicon thin films prepared by pulsed interference laser crystallization (ILC) of amorphous silicon. The 100 nm thin nominally undoped layer was deposited by low pressure chemical vapour deposition (LPCVD) at 560°C on 2 μm of thermal SiO_2 supported by a monocrystalline silicon substrate. For silane dilution, helium was used to avoid explosive hydrogen effusion during laser irradiation. A 50 nm SiO_2 cap layer is grown on top of the amorphous layer to protect it. Laser crystallization was performed in the same setup, which was used for patterning of a–Si:H. The interference pattern had again the period of 5.3 μm, but the total beam energy was 360 mJ/cm^2. Just prior to or after the laser

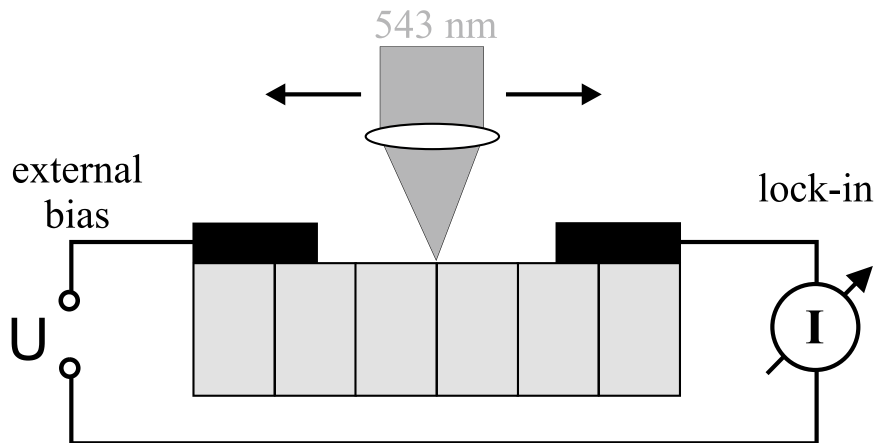

Figure 9: *The scheme of LBIC principle.*

processing the SiO_2 cap layer has been selectively etched away in a buffered solution of hydrofluoric acid. Then titanium/platinum/gold contacts in coplanar configuration were evaporated on the sample in order to characterize its electronic properties.

After LBIC measurement the surface morphology of the sample has been characterized by use of a Digital Instruments AFM operated in the tapping mode. The Secco etching [?] was usually applied to accentuate the grain boundaries in laser crystallized layers.

Single pulse ILC

In the layers crystallized by a single pulse irradiation, the typical grain sizes were smaller than the focus diameter of LBIC probing beam. Therefore the fine structure observed in the LBIC profile could not be directly interpreted as the photoresponse of an individual grain or grain boundary. Nevertheless there was a resemblance between AFM profile of the Secco etched surface with enhanced grain boundaries and LBIC spatial profiles of untreated surface. Although AFM and LBIC spatial profiles were not measured simultaneously, their correlation were interpreted from the Fourier spectra. The photocurrent response to a local focused laser beam excitation was dominated by the variations in the sample thickness, which was much smaller than absorption depth of the light used. The maxima of the photocurrent were correlated with maxima of the surface height. The pronounced surface corrugation was induced by buckling of the SiO_2 cap layer during laser processing [?].

Multiple pulse scanned ILC

To obtain large grains, LBIC response of which could be probed individually, the specific pulsed ILC was applied. Grains of quadratic shape and grain sizes exceeding 5 μm (see Fig. ??) were formed by shifting the sample continuously through the interference pattern, thus taking advantage of lateral epitaxial regrowth [?]. The SiO_2 cap layer was removed just prior to the crystallization so that its buckling was avoided.

To obtain LBIC spatial profiles the sample was scanned by the piezo table with steps of 125 nm distance. The laser beam intensity incidenting on the sample was 40 μW. The generated photocurrent was measured using lock-in detection with a chopping frequency of 41.7 Hz. No external bias was applied to the electrodes and both amplitude and phase of the photocurrent were registered.

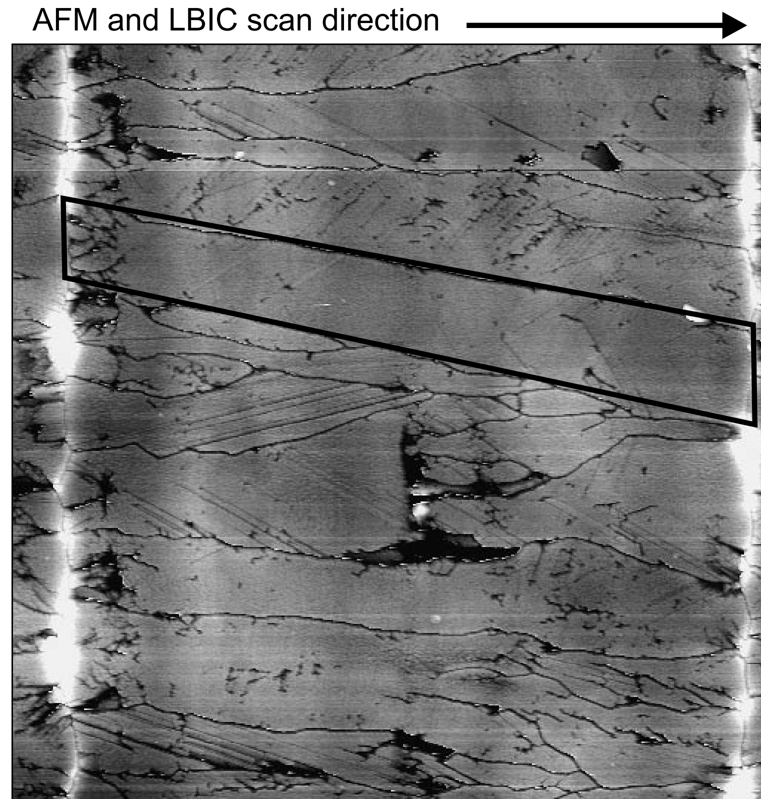

Figure 10: *(a) AFM surface morphology of a polycrystalline silicon thin film prepared by specific interference laser crystallization of amorphous silicon. Grain boundaries have been accentuated by Secco etching. The black rectangle emphasizes one large grain.*

The resulting spatial profiles of photocurrent amplitude (solid) and phase (dashed) are shown in Fig. ??(a) and the section of surface morphology detected by AFM prior to the Secco etching is shown in Fig. ??(b). In the direction of the scan the typical grain size is in the range of 5 μm. The photocurrent shows pronounced fluctuations with similar periodicity. The maxima of photocurrent fluctuations are in close neighbourhood to 180° phase shifts, which indicate sign reversal of the photocurrent.

Since spatially resolved photocurrents as shown in Fig. ??(a) were observed in short circuit mode without application of an external field, the photocurrents are generated by built-in fields, which originate most likely from band bending at grain boundaries [?]. It is interesting to note that within one period (distance between two photocurrent maxima) two phase shifts are observed.

A model for this phenomenon is schematically shown in Fig. ??. On each side of the grain boundary, the electric field is oriented in the opposite direction. As the laser spot approaches the grain boundary from one side, an increasing photocurrent is generated due to the increasing electric field. As soon as part of the light illuminates the other side of the boundary, a photocurrent with opposite sign starts

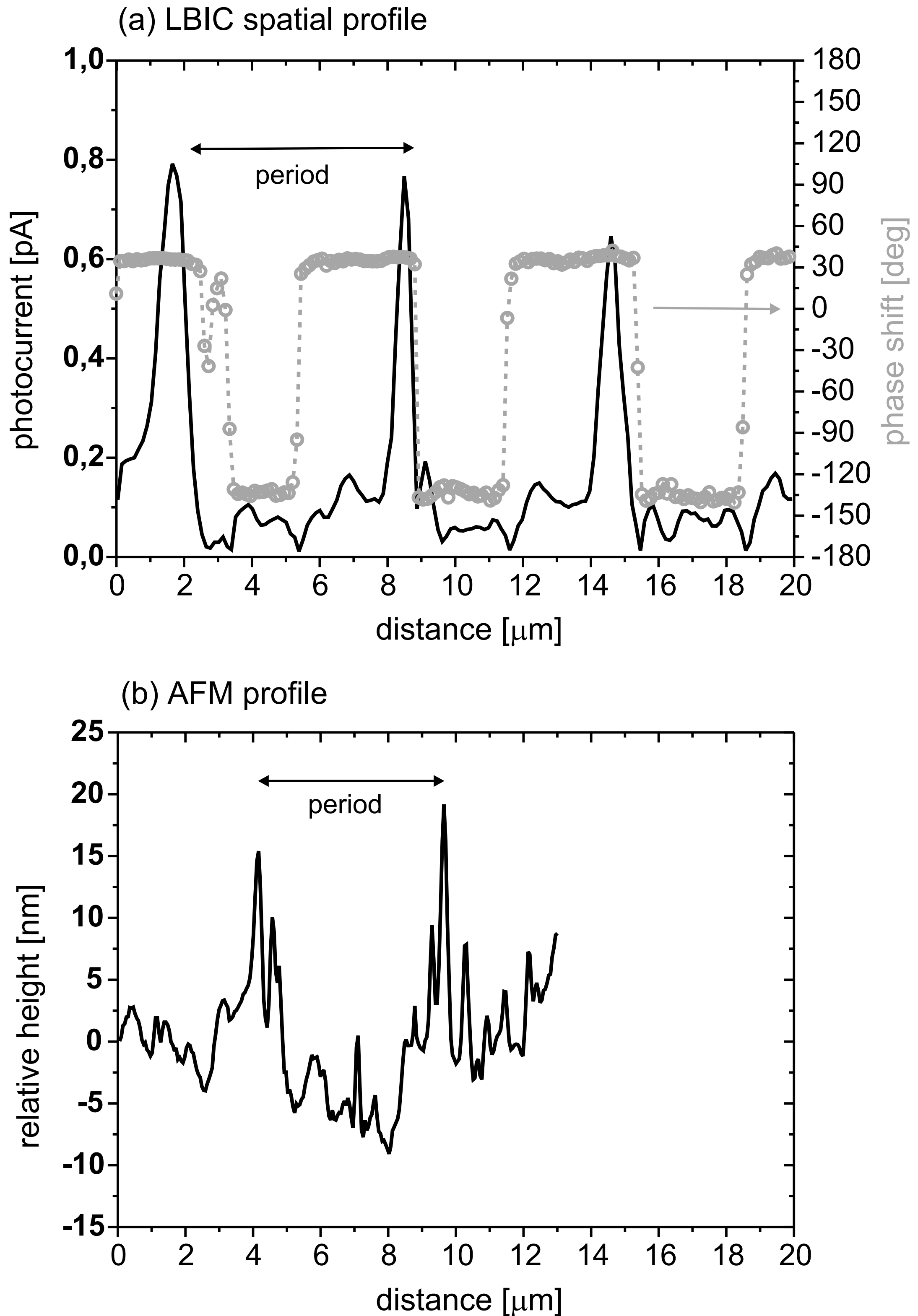

Figure 11: *(a) Spatial variations of the photocurrent (solid line) and of its phase (dashed line). (b) AFM profile of the laser crystallized silicon surface prior to Secco etching. The pronounced peaks are related to grain boundaries. Note that the AFM and LBIC data have been acquired on slightly different spots.*

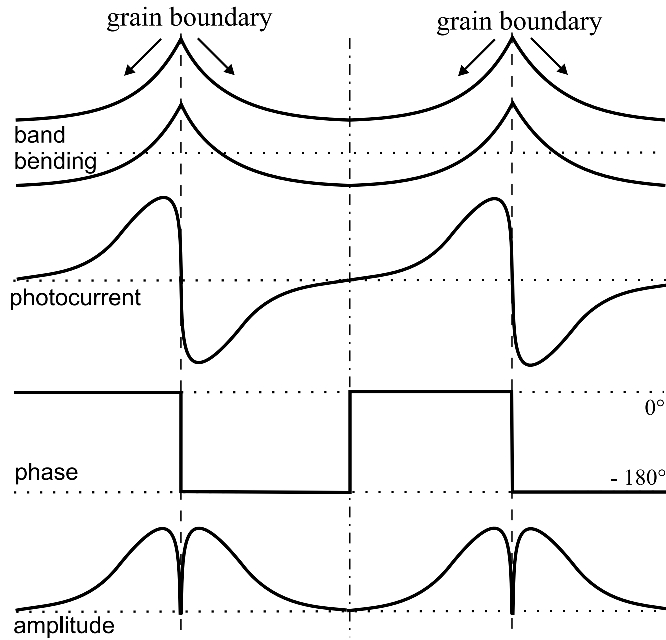

Figure 12: *The model of photocurrent response induced by a laser beam, which scans across two grain boundaries.*

flowing, reducing the effective photoresponse measured by lock-in. When the laser spot illuminates the center of the boundary, both photocurrents are about equal and the resulting current is zero. As the scan continues the photocurrent grows again, however with reversed polarity. Therefore, the phase of the photocurrent at grain boundaries changes by 180°The phase changes again when the laser spot passes the grain center and approaches another grain boundary. Indeed, this double phase shift per period is experimentally detected.

Thus, while the photocurrent is highly sensitive to the local electronic properties, by evaluation of the phase shift of the photocurrent LBIC can reveal with high resolution the positions of grain boundariesin large grained silicon thin films. A phase shift of 180° denotes a reversal of the photocurrent, which is attributed to grain boundary fields and which indicates that grain boundaries are efficient electronic barriers for carrier propagation in the layers.

4. Conclusions

In this work a more light was shed on the connection between the microstructure and local electronic properties of amorphous and microcrystalline silicon thin films. Atomic force microscopy and a technique of light beam induced current were success-

fully applied for this task and revealed pronounced features in electronic transport properties on a microscopic level.

Atomic force microscopy was used to give the picture of a surface morphology and simultaneously registered the current flowing through the layer with very high lateral resolution. Although detailed studies of local current behaviour showed that it is affected by many factors (time, voltage, barriers), the local current was determined predominantly by the material properties. Simultaneous measurement of AFM and local currents allowed direct correlation between surface morphology and local electronic properties of the material. This approach revealed pronounced inhomogeneity of microcrystalline silicon thin films prepared by PECVD technique, resolving details of a few nanometers in size, and made possible a non-invasive evaluation of microscopic patterns produced in silicon thin films by interference laser crystallization, where it has provided a clear and accurate identification of amorphous and microcrystalline parts.

Photoelectrical properties of microcrystalline silicon layers were characterized by the light beam induced current technique with the resolution in the sub-micrometer regime and they were correlated with a surface morphology obtained by atomic force microscopy. In large grained microcrystalline silicon layers produced by specific technology of interference laser crystallization, LBIC was able to detect position and local electronic properties of individual grain boundaries. While the photocurrent was highly sensitive to the quality of local electronic properties of the microcrystalline silicon layers, a clear indication of grain boundaries can be gained by evaluation of the phase shift of the photocurrent. The phase shift of 180° denotes accurately a reversal of the photocurrent at a grain boundary, which indicates that grain boundaries are efficient electronic barriers for carrier propagation in the layers.

A new interesting phenomenon was discovered during the course of this work. In AFM/current measurements a silicon thin film was found to remember that the voltage was applied at a particular place. Although the complete mechanism of this memory effect is still unknown, it may show up as an interesting feature for application in microelectronics and is worth of further investigation.

To conclude, simultaneous AFM/current measurement as well as LBIC technique allowed direct correlation between surface morphology and local electronic properties of silicon thin films with very high lateral resolution. Still some questions remained open and new questions and tasks arose.

List of publications

1. V. Švrček, I. Pelant, J. Kočka, P. Fojtík, B. Rezek, H. Stuchlíková, A. Fejfar, J.Stuchlík, A. Poruba and J. Toušek. *Transport anisotropy in microcrystalline silicon studied by measurement of ambipolar diffusion length.* J. Appl. Phys., **to be published** (2000).

2. A. Fejfar, T. Mates, B. Rezek, J. Stuchlík, V. Vorlíček, K. Drbohlav, I. Pelant and J. Kočka. *Influence of crystallinity and grains on the transport properties of microcrystalline silicon.* Proc. of the 16th European Conf. Photovoltaic Solar Energy Conversion, **to be published** (Glasgow 2000).

3. V. Švrček, P. Fojtík, I. Pelant, B. Rezek, J. Stuchlík, J. Toušek, A. Fejfar and J. Kočka. *Anisotropie mikrokrystalického křemíku - jeho studium pomocí metod SPV a SSPG.* Sborník ze semináře odborné skupiny Polovodiče FVS JČMF, page 13 (Liblice 2000).

4. A. Fejfar, B. Rezek, J. Stuchlík, H. Stuchlíková, V. Švrček, P. Fojtík, T. Mates, I. Pelant and J. Kočka. *Transport elektrického náboje v mikrokrystalickém křemíku pro sluneční články.* Sborník ze semináře odborné skupiny Polovodiče FVS JČMF, page 84 (Liblice 2000).

5. B. Rezek, C. E. Nebel and M. Stutzmann. *Interference laser crystallization of microcrystalline silicon using asymmetric beam intensities.* J. Non-crystal. Solids, **266 - 269**, 650 (2000).

6. B. Rezek, C. E. Nebel and M. Stutzmann. *Local photoconductivity correlation with granular structure of microcrystalline silicon thin films.* J. Non-crystal. Solids, **266 - 269**, 315 (2000).

7. A. Fejfar, B. Rezek, P. Knápek, J. Stuchlík and J. Kočka. *Local electronic transport in μc-Si:H observed by combined AFM measurements.* J. Non-crystal. Solids, **266 - 269**, 309 (2000).

8. B. Rezek, C. E. Nebel and M. Stutzmann. *Polycrystalline silicon thin films produced by interference laser crystallization of amorphous silicon.* Jpn. J. Appl. Phys., **38**, L1083 (1999).

9. B. Rezek, C. E. Nebel and M. Stutzmann. *Correlation of photoconductivity and structure of microcrystalline silicon thin films with submicron resolution.* Appl. Phys. Lett., **75**, 1742 (1999).

10. B. Rezek, J. Stuchlík, A. Fejfar and J. Kočka. *Local characterization of electronic transport in microcrystalline silicon thin films with submicron resolution.* Appl. Phys. Lett., **74**, 1475 (1999).

11. J. Kočka, A. Fejfar, B. Rezek, H. Stuchlíková, J. Stuchlík, V. Švrček and P. Fojtík. *Progress in characterization of transport in microcrystalline silicon.* Tech. Digest of the Review meeting for research with overseas country research institutes, page 33 (Tokyo 1999).

12. C. E. Zybill, H. Boubekeur, P. Radojkovic, M. Schwartzkopff, E. Hartmann, F. Koch, G. Groos, B. Rezek, R. Bruchhaus and W. Wersing. *Direct observation of single domains in poled (111) PZT ($PbZr_{0.25}Ti_{0.75}O_3$) films*. Surface Science, **440**, 221 (1999).

13. B. Rezek, J. Stuchlík, A. Fejfar and J. Kočka. *Characterization of laser patterned a-Si:H thin films by combined AFM/local current measurements*. phys. stat. sol. (a), **170/1**, R1 (1998).

14. P. Knápek, B. Rezek, D. Muller, J. J. Grob, R. Lévy, K. Luterová, J. Kočka and I. Pelant. *Blue electroluminiscence from an SiO_2 film highly implanted with Si^+ ions*. phys. stat. sol. (a), **167**, R5 (1998).

15. J. Kočka, A. Fejfar, H. Stuchlíková, B. Rezek, A. Poruba, M. Vaněček, P. Torres, J. Meier, N. Wyrsch, A. Shah and A. Matsuda. *Charge transport in microcrystalline silicon, relation to thin film solar cells*. Proc. of the 2nd World Conf. Photovoltaic Solar Energy Conversion, page 785 (Vienna 1998).

16. A. Fejfar and B. Rezek. *Thin nanocomposite films of phthalocyanines and metals*. Vacuum, **50**, 191 (1998).

17. B. Rezek, M. Trchová and A. Fejfar. *Nanostructural composites of phthalocyanines and metals*. Czechoslovak J. Physics, **47**, 461 (1997).

18. I. Ohlídal, D. Franta, B. Rezek and M. Ohlídal. *Analysis of single layers placed on slightly rough surfaces by spectroscopic ellipsometry, spectroscopic reflectometry and atomic force microscopy*. Proc. of the 7th European Conference on Applications of Surface and Interface Analysis, page 1051 (Gőteborg 1997).

19. A. Fejfar, B. Rezek and M. Trchová. *Tenké vrstvy nanokompozitů ftalocyaninu a kovu*. Sborník příspěvků 12. konference českých a slovenských fyziků, 502 (Ostrava 1996). (editoři M. Lesňák, J. Luňáček, J. Pištora).

20. A. Fejfar, P. Kroh, B. Rezek, M. Trchová and J. Hála. *Nanostructural composites of phthalocyanines and metals*. Presented at Post-Easter Topical Minisympozium on Optical and Electrical Properties of Organic Solids (Prague 1995).

Author's contribution to the thesis

In the theoretical part the author of this thesis presented a brief overview of local probe techniques suitable for characterization of local transport properties as well as summarized properties of amorphous and microcrystalline silicon with a view to their basic electronic properties.

To the experimental part dealing with combined AFM/current technique the author contributed by AFM/current measurements and laser structuring of PECVD samples, which were prepared by Ing. J. Stuchlík. CPM spectra were measured by V. Švrček and Raman spectra were provided by K. Luterová.

In the part concerning LBIC technique the author performed interference laser crystallization of amorphous silicon films provided by Ing. J. Stuchlík and other sources. The author characterized these samples in the LBIC setup, which was build up by C. Eisele. The author made some modifications and enhancements to the setup and took part in software development.

The author prepared publications 5, 6, 8, 9 in a cooperation with Dr. C. E. Nebel and publications 10, 13, 17 in a cooperation with Dr. A. Fejfar. The author took part in experiments presented in the rest of listed publications.